Proceedings World Geothermal Congress 2015
Melbourne, Australia, 19-25 April 2015

Characterization of Nanocolloidal Silica Formation of Untreated and Treated Simulated Geothermal Brine through Various Particle Size and Zeta Potential Measurement Techniques

Richard C. de Guzman, Al Christopher C. de Leon, Brylee David B. Tiu, Almario D. Baltazar Jr., Rigoberto C. Advincula

Mailing address, Energy Development Corporation, One Corporate Center, Ortigas Center, Pasig City, Philippines 1605

E-mail address, deguzman.rc@energy.com.ph

Keywords: chemical inhibition, particle size, scaling, silica

ABSTRACT

Silica scaling remains to be a major restriction for geothermal heat extraction and continuous operation. Numerous studies have been conducted both in the laboratory and in the field but the microscopic-level mechanism of growth, transport and attachment has not been investigated extensively and is not yet fully understood. Thermodynamic evaluation, through the calculation of silica saturation indices, could be further refined by macromolecular characterization techniques on the early polymerization phase, or the nanocolloidal silica formation. This study evaluates the capability of various particle's size and electrokinetic potential measurement techniques to examine the possibility of silica scaling of simulated geothermal brine at fixed room temperature. In addition to the standard silicomolybdate tests, the brine were subjected to evaluation by obtaining the particle's zeta potential and hydrodynamic radius in solution thru dynamic light scattering (DLS), and apparent height thru atomic force microscopy (AFM), and transmission electron microscopy (TEM). The information gathered and correspondence could expand the understanding of silica scaling, and present opportunities for improved inhibition technologies. These techniques were extended to evaluate available chemical inhibition techniques, and the nanocolloidal silica profile comparisons could refine the application of such technologies. Mechanisms of inhibition by different types of cationic and anionic inhibitors were also studied.

1. INTRODUCTION

Geothermal technology proves to be a reliable and sustainable source of energy since the commissioning of the first ever power plant in Larderello, Italy in 1904. Numerous milestones have led to improved and deeper understanding on exploration, drilling, geochemistry and reservoir engineering. However, full utilization of the geothermal fluid's energy is hampered by several factors like the formation of silica scales (mostly amorphous silica). This manifests thru the conductive cooling of the fluid, effectively decreasing the solubility of silica and the subsequent removal of steam from the fluid which further increases the concentration of the silica in the liquid portion as discussed by Brown (2011). Heat extraction in the system is maximized based on the amorphous silica solubility behavior, illustrated in Figure 1 by Angcoy (2006). In Figure 1, geothermal operations must be maintained within the no silica scaling zone to avoid massive deposition problems leading to reduced fluid flow, or at the worst, total blockage. Depositions could occur anywhere in the system, from the production wells, two-phase headers, separator vessels, brine lines and reinjection lines. There are cases where silica deposits where found even in steam lines and turbine equipment. Silica scaling has been identified as the primary hindrance to efficient geothermal heat extraction by Gunnarson and Arnorsson (2003).

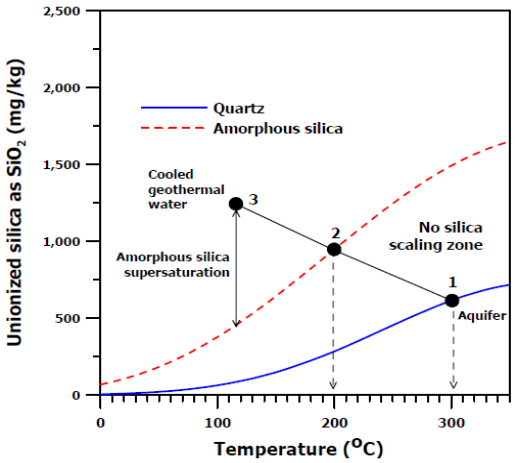

Figure 1: Geothermal fluid extraction pathway compared with quartz and amorphous silica saturation lines (Angcoy 2006).

Silica is a general term commonly referred to the compound silicon dioxide (SiO_2) and has a number of polymorphs from its most crystalline (quartz) to its most disordered (amorphous silica). However, silica in solution is in the forms of SiO_4 more commonly referred to as silicic acid or monomeric silica. It has a tetrahedral formation with -Si-O- bond partially ionic in character. A simple molecular model can be seen in Figure 2.

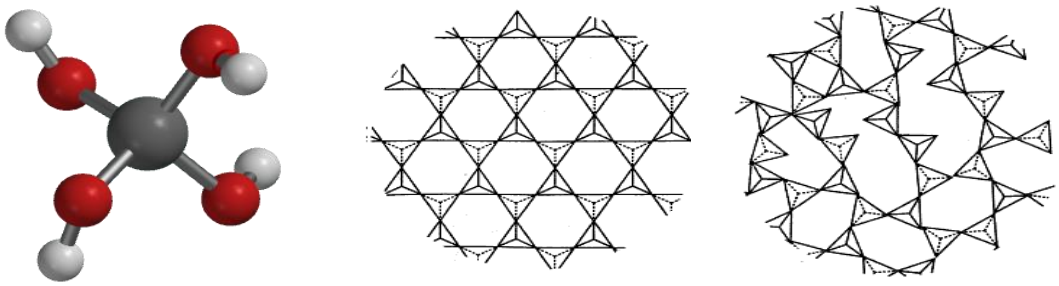

(a) **(b)** **(c)**

Figure 2: Molecular models of (a) silicic acid or monomeric silica, (b) crystalline silica formation and (c) amorphous silica formation summarized by Iler (1979).

The formation of amorphous silica scales is known to occur via three mechanisms: (1) direct deposition or monomeric deposition, (2) colloidal deposition, and (3) biogenic deposition but for geothermal applications, the last one is not a major concern. The first one, direct deposition depends on the interaction of siloxane bonds of the silicic acid to the metal surface. This reaction is known to usually occur at high pH levels (pH > 8) and is catalyzed by hydroxyl ions. This produces a hard, dense and vitreous layer estimated to be contributing 0.5mm/yr of scale, an estimate by Sinclair (2012). On the other hand, colloidal deposition occurs via a condensation-polymerization mechanism from silicic acid due to increasing saturation/supersaturation. This formation pathway forms small molecular weight dimers and trimers prior to forming rings of various sizes, and cross-linked polymeric chains and ultimately a complex and amorphous product as discussed by Amjad (2010). This study is focused on colloidal deposition, more specifically, the nanocolloidal silica formation. The process of scale formation from silica monomers can be summarized from Figure 3, Bergna and Roberts (2006). After the polymerization stages, coagulation and flocculation further promotes the formation of much larger colloid particles.

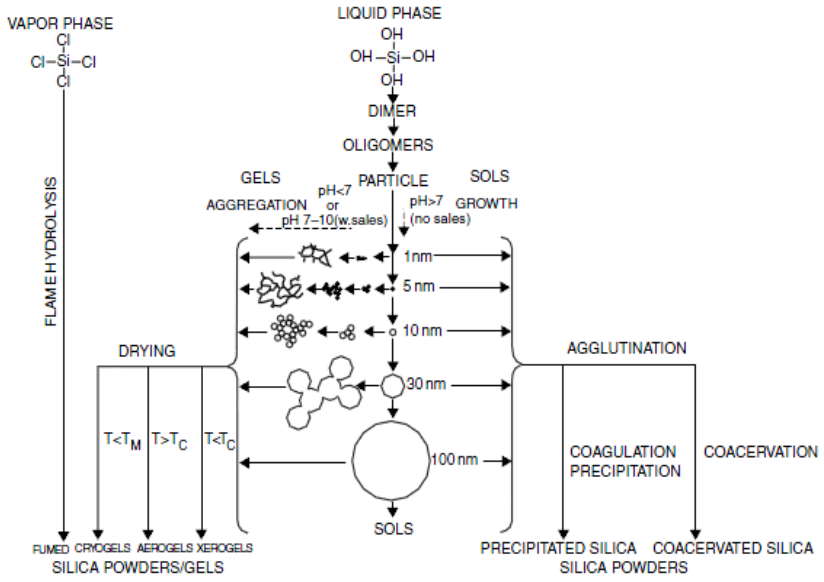

Figure 3: Condensation polymerization pathways from monomeric silica by Bergna and Roberts (2006).

Brown (2011) discussed that deposition is mainly affected by the silica concentration, temperature and pH but flow rates, aeration and ion effects are also important factors. Monitoring of the likelihood of scaling is measured thermodynamically using the calculation of the silica saturation index or the SSI. This is a ratio of the monomeric silica measured in solution and the equilibrium silica concentration in the solution. The latter was calculated by Fournier (1977) from an empirical model based on silica measurement versus temperature. An SSI of unity (1.0) means that the fluid has reached equilibrium saturation level and any increase in concentration promotes the precipitation. However, this is a thermodynamic measurement alone and does not include kinetic or flow effects.

Primarily, the operating conditions are maintained at the no scaling zone. Numerous mitigation measures have been tested and these are summarized as follows: addition of silica scale inhibitors and dispersant dilution of the brine with freshwater, pH reduction to reduce the kinetics of polymerization, addition of dispersing/inhibiting agents to prevent silica side-reactions, removal of silica via induced precipitation, and cooling or rapid thermal quenching as discussed by Sinclair (2012). Energy Development Corporation (EDC) has experimented on several inhibitors and has used phosphino-carboxylic acid copolymer for ultra-high silica levels as experienced by Baltazar et al (1997) and during the recent low-temperature medium-term discharge conducted by de Guzman et al (2013). However, the full microscopic-level mechanism of inhibition was not fully understood yet.

This research project was designed to improve the understanding of the silica scaling phenomena in geothermal fluid using modern nanocolloidal particle size measurement techniques of the untreated and the treated simulated geothermal brine at room temperature. These were aimed to gain new insights on the characterization of the silica oligomerization leading to scaling, the evaluation of current chemical inhibition technologies and the evaluation of new methods for the early detection of silica scaling.

2. EXPERIMENTAL DESIGN

2.1 Project Objectives

This research was aimed to better understand the silica scaling phenomenon in geothermal fluid by looking at the particle formation behavior measured in solution and upon deposition on a solid substrate. The information gathered from the old and new techniques are used to (1) characterize the silica oligomerization (or the nanocolloid formation) process leading to scaling, (2) evaluate inhibition technologies and (3) look for improved methods on the early detection of scaling.

2.2 Experimentation and Testing

At room temperature, two solutions were used to recreate the brine chemistry of one of the scaling wells in EDC. Silica solutions were prepared from $Na_2SiO_2 \bullet 5H_2O$ passed through cation exchange resins and kept in plastic containers while the rest of the brine was prepared from reagent-grade salts. The two solutions were mixed to achieve the target brine chemistry and pH corrected to neutral levels (7.0-7.5) identified as the zone of minimum silicic acid solubility as coined by Amjad (2010). Different variations of the solutions were prepared to account for the effects of such variables to silica formation. In addition, different inhibitor treatments were used in the samples. Three inhibitors were tested in this project: two were identified as sodium salts of polycarboxylic acid while the third was a mixture with less than 50% carboxylic acid. Limited information with regards to chemical identity, composition and properties were available.

Several tests were used including the conventional molybdate-reactive silica concentration tests (guided by ASTM D859-00), particle size measurement tests (atomic force microscopy or AFM, dynamic light scattering or DLS and transmission electron microscopy or TEM) and zeta potential meter. For silica deposited on a solid substrate, mica was used in testing using the AFM while the standard grid was used for the TEM.

3. RESULTS AND DISCUSSION

Blank or freshly exfoliated mica substrates were scanned using the optical microscope and the AFM shown in Figure 4. These are baseline surfaces, showing a clean surface with height profiles almost negligible. Height profiles manifested by the histogram of the number of pixels per measured levels was standardized and used to provide a measure of the most dominant height levels of the silica nanoparticles on the substrate. From these scans, mica manifested a height distribution of 1-2 nm. These height levels are negligible compared to the sample scans obtained.

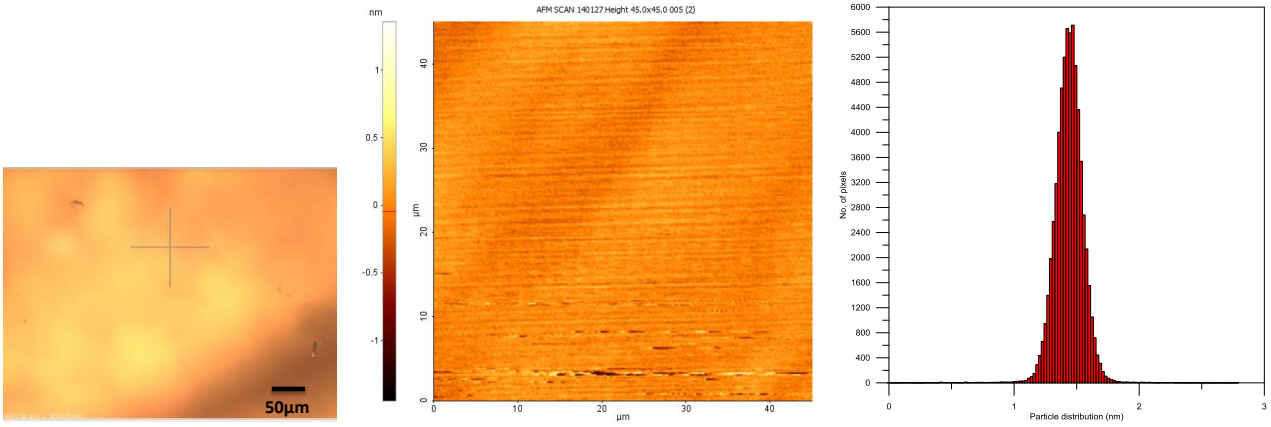

(a) **(b)** **(c)**

Figure 4: Fresh mica surface scans using different methods using (a) optical microscopy, and from AFM scan (b) height profile and (c) height distribution.

Since the methods are new and untested on this scope, the techniques mentioned were applied on simulated fluid with a very high silica saturation level. The chemistry used was similar to that of actual brine but the testing at room temperature increased the supersaturation to up to 6.0-6.5. The untreated highly supersaturated solution tended to re-arrange to a film-like formation apparent to both the optical and the AFM image in Figure 5. This filming effect is consistent with the stipulations of Iler (1979)

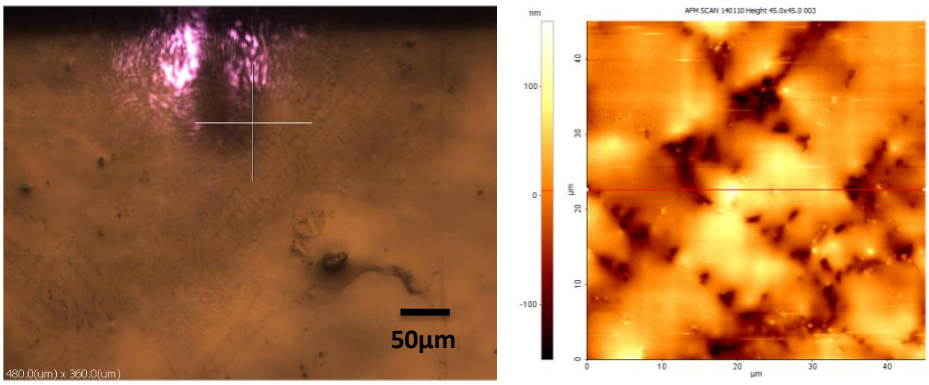

(a) **(b)**

Figure 5: Highly supersaturated brine solution (SSI 6.0-6.5) (a) optical and (b) AFM images.

In addition, transmission electron microscopy (TEM) scans were conducted and the results showed several large particles and the rest is a more uniform set of smaller particles. The scans are presented in Figure 6.

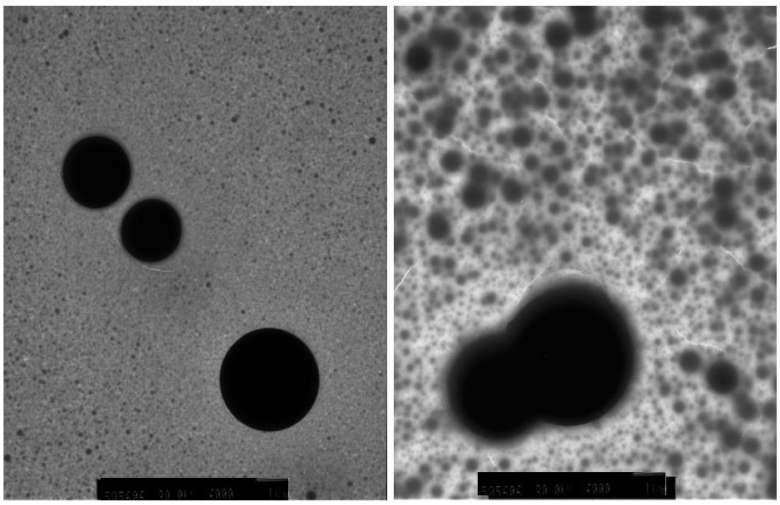

Figure 6: TEM scans of highly supersaturated brine.

The test brine's saturation levels were then benchmarked based on the field SSI rather than the silica levels itself. Silica levels were then maintained at twice the saturation level alone (room temperature conditions), while the other ions (cations/anions) were kept at the same levels. Another variable was also added and that is the presence of iron in the solution. The model brine fluid has very little to no iron, but the corrosion in the pipes could supply ferric ions in the solution. The first set of images in Figure 7 and 8 includes the simulated brine with no iron content, untreated and treated.

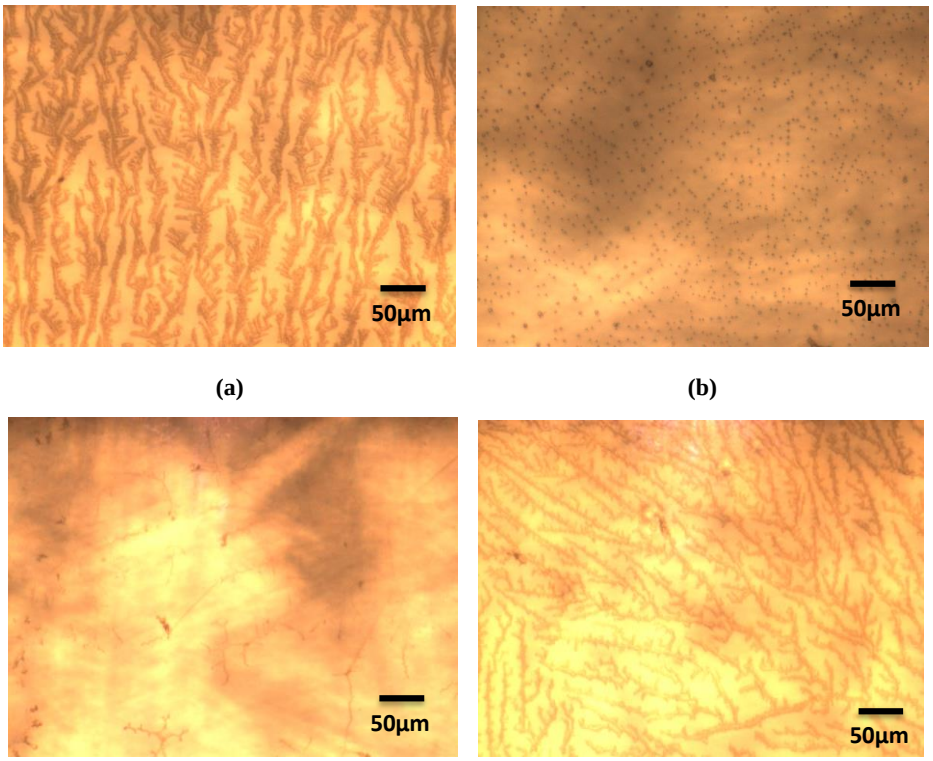

(a) **(b)**

(c) **(d)**

Figure 7: Optical images of tested brine (no iron content) with SSI 2.0 for (a) untreated and treated samples (b) Inhibitor 1 (c) Inhibitor 2 and (d) Inhibitor 3.

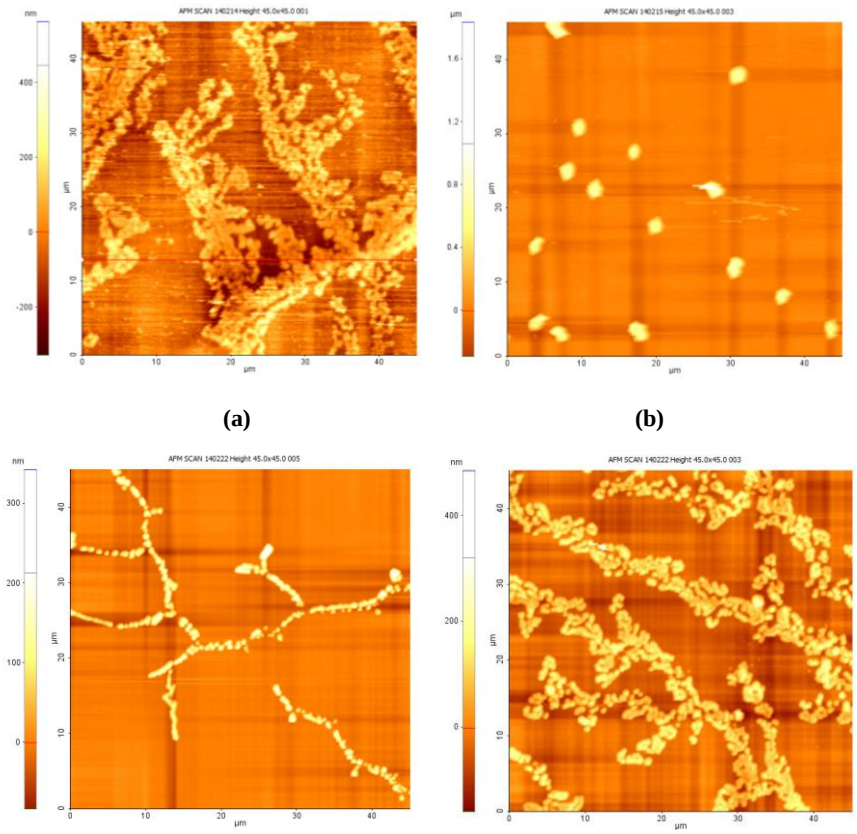

(a) **(b)**

(c) **(d)**

Figure 8: AFM images of tested brine (no iron content) with SSI 2.0 for (a) untreated and treated samples (b) Inhibitor 1 (c) Inhibitor 2 and (d) Inhibitor 3.

These images confirm the theories of polymeric formation mentioned earlier. To summarize, the process replicates the images presented by Iler (1979). In terms of inhibition effectivity, the usual practice is to measure the molybdate-reactive silica, previously known as the monomeric silica but later expanded to include dimers, trimers chain and cyclic tetramers and that definition is applied similarly here. For the simulated brine's silica levels shown in Figure 9, all three inhibitors seemed to be effective since the treated samples are higher than the untreated samples and these profiles were compared to the height profiles measured from the AFM scans.

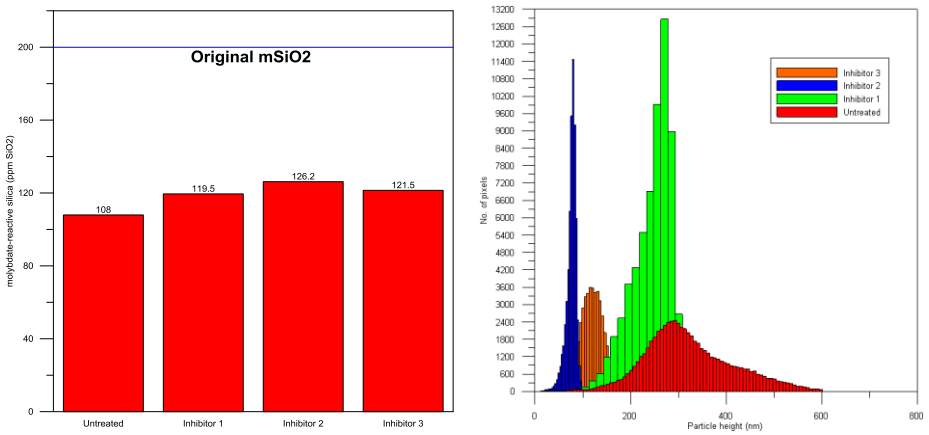

(a) **(b)**

Figure 9: (a) Oligomeric silica levels measured by colorimetric methods and (b) particle height distribution from AFM scans.

The addition of the height profiles from the same set of samples further refine what was generalized by the molybdate-reactive silica testing. Focusing on the height profiles, the measured heights were shifted to the right with the smallest particles formed by Inhibitor 2. Inhibitors 1 and 3 were a little higher. In addition, the dynamic light scattering (DLS) technique was used to monitor the particle size distribution in solution. The particles' hydrodynamic radius is the one being measured in the solution. The results are summarized in a bubble plot shown in Figure 10. This figure presents the information provided by DLS scans which include the percent mass distribution in the y-axis of the various hydrodynamic radii of particles in the solution (visualized and labeled in plot, noted above particle). The plot also separates per treatment (untreated, inhibitors 1, 2 and 3).

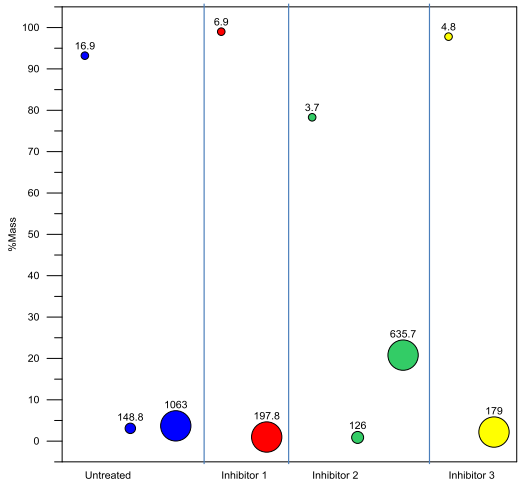

Figure 10: Dynamic light scattering (DLS) particle distribution for untreated and treated samples.

Figure 10 shows a major difference between inhibitors 1 and 3 compared to that of Inhibitor 2. The former's mechanism seems to be focused on maintaining the silica in its monomeric or a more accurate description is its oligomeric form. It is also noteworthy to compare the distribution of the untreated with its biggest particle at 1µm while the treated particles were significantly lower. These were consistent to reported mechanism modes of cationic and anionic inhibitors. Inhibitors 1 and 3 are postulated to be anionic inhibitors while Inhibitor 2 is cationic in nature. The mechanisms are better summarized in the Figure 11.

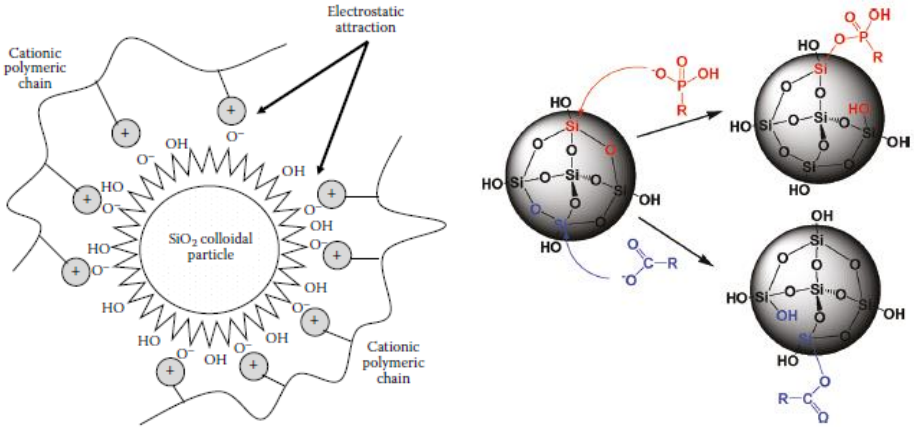

(a) **(b)**

Figure 11: Silica inhibition mechanisms for (a) cationic by Bergna and Roberts (2006) and (b) anionic polymers by Demadis et al (2011).

Cation polymers/inhibitors attack the silicic acid monoanion and is fundamentally an electrostatic interaction to stabilize the ion and the flocculation of the inhibitor and the negatively charged anion as discussed by Bergna (2006). On the other hand, anionic inhibitors act on adsorption on the crystal plane of a seeding nucleus. This stops the growth and agglomeration of the oligomers. This is a sound explanation why Inhibitor 2 does tend to maintain the small oligomers over that of the anionic inhibitor. In addition, the flocculation of the cationic inhibitor with the silica anion could further increase the particles hydrodynamic radius size compared to the others. On the other hand, the addition of an excess of 10ppm ferric ions in brine resulted to different results and trends compared to that of the simulated brine. There is a distinct difference in the morphology and particle size profiles. The AFM scans are presented in Figure 12 and 13.

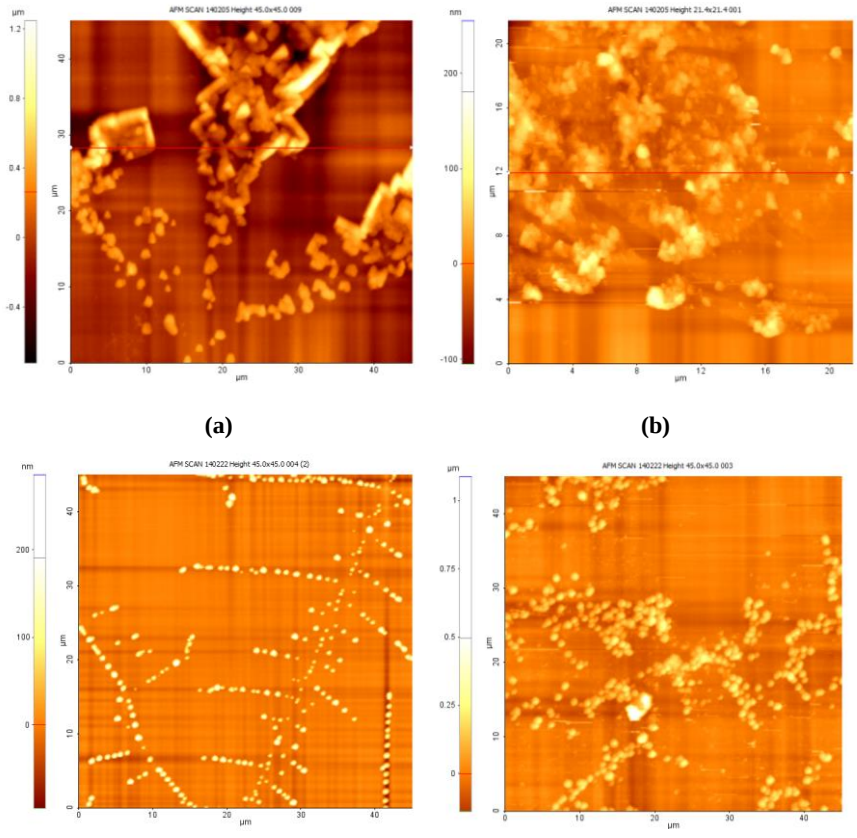

(a) **(b)**

(c) **(d)**

Figure 12: AFM images of tested brine (with 10ppm iron content) with SSI 2.0 for (a) untreated and treated samples (b) Inhibitor 1 (c) Inhibitor 2 and (d) Inhibitor 3.

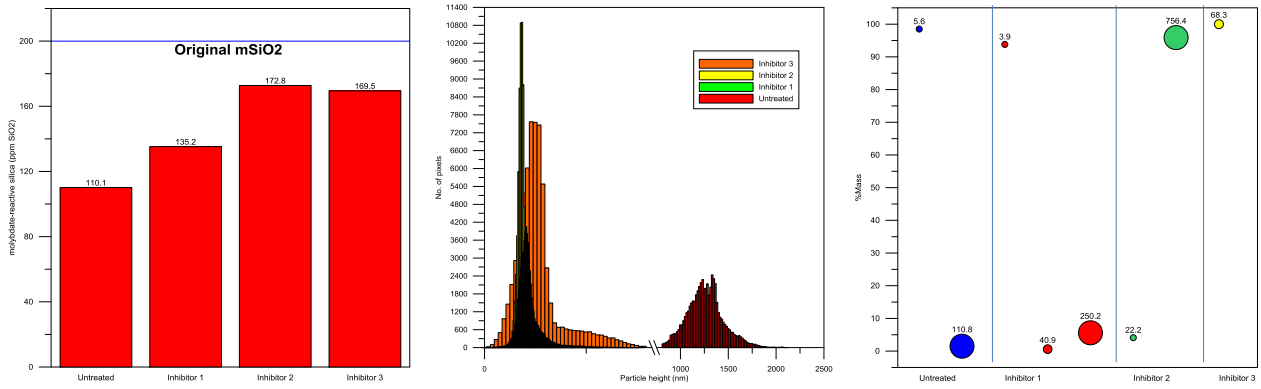

(a) **(b)** **(c)**

Figure 13: Profiles for (a) molybdate-reactive silica, (b) height profile from AFM scans and (c) DLS radius distribution for simulated brine with 10ppm Fe.

Zeta potential is a common field of measure for colloidal chemistry. It is known that silica in solution has a negative zeta potential charge but this is dependent on the pH of the solution. The presence of cations and anions in solution could also shift the charge of the zeta potential. In this test, the measure of the solutions conductivity was used to qualify the measured zeta potential. Error bars are also included in the plots.

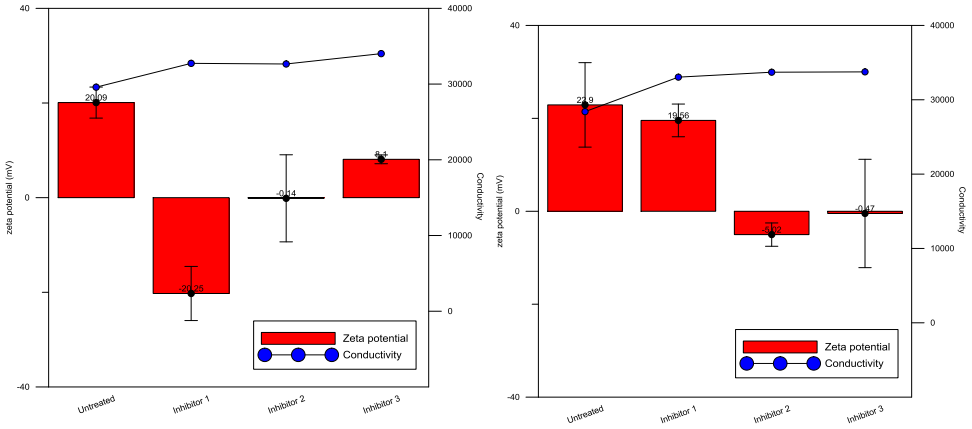

(a) **(b)**

Figure 14: Zeta potential and conductivity measurements for simulated brine with (a) no Fe and (b) 10ppm Fe.

4. CONCLUSION AND RECOMMENDATIONS

A new set of characterization techniques were used in the analysis of the formation of silica nanocolloids and the corresponding effect of chemical inhibitors. In addition to the measurement of silica-molybdate colorimetric techniques, particle sizes upon settling on a surface were measured using the optical microscope, atomic force microscopy (AFM), and the transmission electron microscopy (TEM). In solution, hydrodynamic radius was measured using the dynamic light scattering (DLS) which can be coupled by the zeta potential and conductivity measurements. These methods could also provide information on the degree of aggregation by referring to particle height distributions.

At neutral pH and laboratory conditions, all three inhibitors tested were effective in terms of maintaining a higher level of oligomeric silica in solution. In addition, the presence of high levels of ferric ions seemed to increase the efficiency of two of the inhibitors tested. This behavior highlights the need to evaluate scaling tendencies not only based on silica concentration and temperature but the competing interaction occurring in high ion content brine.

These methods can be used for improved evaluation of scaling indices and probability by the consideration of particle size measurements in solution and upon adhesion to surface and the consideration of full brine chemistry for scaling evaluations. In addition, this could be used for dosing optimization studies.

ACKNOWLEDGEMENTS

We gratefully acknowledge the technical support from Dr. E. Karathanasis and group from the Biomedical Engineering Department, Dr. S. Rowan and group, Katrina Pangilinan and Joey Mangadlao of the Macromolecular Science and Engineering Department and the School of Medicine of Case Western Reserve University and Park Systems.

REFERENCES

Amjad, Z.: The Science and Technology of Industrial Water Treatment, Boca Raton, Florida: *Taylor & Francis Group*, LLC (2010).

Angcoy, E.: An Experiment on Monomeric and Polymeric Silica Precipitation Rates from Supersaturated Solution, *Geothermal Training Programme*, The United Nations University, **5**, (2006).

Baltazar, A., Garcia, S., Solis, R., and Jordan, O.: Silica Scale Inhibition Experiments: Geogard SX Application on Geothermal Brine With Ultra High Concentration of SiO_2, *Meeting the Challenge of Increased Competition*, Geothermal Resources Council, (1997), 43-48.

Bergna, H., and Roberts W.: Colloidal Silica: Fundamentals and Applications, Boca Raton, Florida: *CRC Press*, (2006).

Brown, K.: Thermodynamics and kinetics of silica scaling, *International Workshop on Mineral Scaling*, Manila (2011).

de Guzman, R., See, F., Baltazar, A., and Salonga, N.: Silica Scale Inhibition by Phosphino-carboxylic Acid Copolymer in Low-temperature Injection of Geothermal Fluid, Tagaytay City, Philippines: *Asian Geothermal Symposium*, (2013).

Demadis, K., Somara, M. and Mavredaki, E.: Additive-Driven Dissolution Enhancement of Colloidal Silica, 1. Basic Principles and Relevance to Water Treatment, *Industrial and Engineering Chemistry Research*, (2011), 12587-12595.

Fournier, R.: The solubility of amorphous silica in water at high temperatures and high pressures, *American Mineralogist*, **62**, (1977), 1052-1056.

Fournier, R. and Potter, R.: A revised and expanded silica (quartz) geothermometer, *Geothermal Resources Council*, **11-10**, (1982).

Gunnarson, I. and Arnorsson S.: Silica scaling: The main obstacle in efficient use of high-temperature geothermal fluids, *International Geothermal Conference*, (2003), 30-36.

Sinclair, L.: Development of a Silica Scaling Test Rig, *University of Canterbury*, (2012).